Hunting long-lived gluinos at the Pierre Auger Observatory

Luis A. Anchordoqui,[1] Antonio Delgado,[2,3] Carlos A. García Canal,[4,5] and Sergio J. Sciutto[4,5]

[1]*Department of Physics, University of Wisconsin-Milwaukee, P.O. Box 413, Milwaukee, Wisconsin 53201, USA*
[2]*CERN, Theory Division, CH-1211 Geneva 23, Switzerland*
[3]*Department of Physics, University of Notre Dame, Notre Dame, Indiana 46556, USA*
[4]*Departamento de Física, Universidad Nacional de La Plata, C.C.67, La Plata (1900), Argentina*
[5]*IFLP (CONICET), Universidad Nacional de La Plata, C.C.67, La Plata 1900, Argentina*

(Received 6 October 2007; published 31 January 2008)

Eventual signals of split supersymmetry in cosmic ray physics are analyzed in detail. The study focuses particularly on quasistable colorless *R*-hadrons originating from confinement of long-lived gluinos (with quarks, antiquarks, and gluons) produced in pp collisions at astrophysical sources. Because of parton density requirements, the gluino has a momentum which is considerably smaller than the energy of the primary proton, and so production of heavy (mass $\sim$500 GeV) *R*-hadrons requires powerful cosmic ray engines able to accelerate particles up to extreme energies, somewhat above $10^{13.6}$ GeV. Using a realistic Monte Carlo simulation with the AIRES engine, we study the main characteristics of the air showers triggered when one of these exotic hadrons impinges on a stationary nucleon of the Earth's atmosphere. We show that *R*-hadron air showers present clear differences with respect to those initiated by standard particles. We use these shower characteristics to construct observables which may be used to distinguish long-lived gluinos at the Pierre Auger Observatory.

DOI: 10.1103/PhysRevD.77.023009 PACS numbers: 96.50.sd, 11.30.Pb, 13.85.Tp

I. INTRODUCTION

There exists ''lore'' that convinces us that physics beyond the standard model (SM) should be guided from the stabilization of mass hierarchy. The most ubiquitous example is the minimal low energy effective supersymmetric theory (MSSM) [1], which requires a scale of supersymmetry (SUSY) breaking $\Lambda_{\rm SUSY} \sim 1$ TeV to avoid the fine-tuning problem ($f_{\rm lore} \sim M_H^2/\Lambda_{\rm SUSY}^2$) with the Higgs mass ($M_H \sim 100$ GeV). However, this ''naturalness'' is not favored by precision tests at colliders, which are consistent with SM to a great accuracy [2]. Consequently, any new physics which may turn on beyond the electroweak scale needs to be fine-tuned at the percent level. Moreover, the presence [3] of a tiny, but nonvanishing, cosmological constant presents us with a fine-tuning problem much more severe than the gauge hierarchy problem.

The last resort to address the cosmological constant problem is Weinberg's anthropic approach [4], in which there exists an enormous ''landscape'' of vacua, only a small fraction of which have a vacuum energy small enough to allow for a natural habitat for observers such as ourselves. This approach has recently been rekindled by investigations in string theory which have applied a statistical analysis to the large number N of vacua in the theory [5]. Among this vast number of metastable vacua, there can be a small subset $\mathcal{O}(10^{40})$ exhibiting low-scale SUSY breaking. Of course, the fine-tuning required to achieve a small cosmological constant implies the need for a huge number of vacua, far more than the $\mathcal{O}(10^{40})$ characterizing low-scale SUSY breaking. However, the density of vacua increases $\propto \Lambda_{\rm SUSY}^{2N}$ [6]. Therefore, assigning *a priori* equal probability to each vacuum, one arrives at a new measure of fine-tuning, which takes into account the ''entropy'' associated with the density of vacua, $f_{\rm new} \sim M_H^2 \Lambda_{\rm SUSY}^N$. Contrary to $f_{\rm lore}$ requirements, $f_{\rm new}$ clearly favors a large SUSY breaking scale. For example, for $\Lambda_{\rm SUSY} \sim 10^{10}$ GeV, $\mathcal{O}(10^{200})$ vacua become available, enough to fine-tune both the cosmological constant and the Higgs mass. If we live in this neighborhood of the landscape, collider data would be expected to point to the SM rather than SUSY. However, one pays a price for throwing away MSSM, since it provides a potential explanation for both dark matter [7] and the LEP results favoring the unification of the three SM gauge couplings [8].

Split SUSY [9] is a relatively new variant of SUSY which may facilitate the required fine-tuning and simultaneously preserves the achievements of the MSSM. In this model the bosonic superpartners are heavy, while the extra fermions retain TeV-scale masses thanks to protection by chiral symmetry. Although split SUSY does not provide a dynamical explanation for the hierarchy problem, the assumption of large-scale SUSY breaking leads to important information on the underlying parameters and on measurable physical quantities [10]. In particular, analyses of one loop [11] and two loop [12] running of the RG equations show that split SUSY preserves unification of couplings. Additionally, as in the MSSM, the lightest supersymmetric particle provides a possible candidate for cold dark matter [13].

It is clear that split SUSY opens new territory for model builders; gauginos have a symmetry that protects their masses, namely, the *R*-symmetry, so building models where scalars are very massive is quite natural in theories where this symmetry is not broken, for example, in *D*-term breaking models; it can also happen in theories with extended supersymmetries, and there are already several

 © 2008 The American Physical Society

papers with string inspired models of split SUSY [14]. Hence there is a strong motivation for phenomenological studies, including implications for collider-based measurements [15–17], electric dipole moments [18], Higgs physics and electroweak symmetry breaking [19], and cosmic ray physics [16,20,21]. The latter is the main focus of the present study.

An intriguing prediction of split SUSY, which represents a radical departure from the MSSM, is the longevity of the gluino. As mentioned above, in split SUSY the squarks are very massive so gluino decay via virtual squarks becomes strongly suppressed, yielding a $\tilde{g}$ lifetime of the order of [9]

$$\tau_{\tilde{g}} \simeq 3 \times 10^{-2} \left(\frac{\mathrm{TeV}}{M_{\tilde{g}}}\right)^5 \left(\frac{\Lambda_{\mathrm{SUSY}}}{10^9\ \mathrm{GeV}}\right)^4 \mathrm{s}, \qquad (1)$$

where $M_{\tilde{g}}$ is the gluino mass. Quasistable colorless R-hadrons (i.e., carrying one unit of R-parity) are expected to be born when such long-lived gluinos become confined with quarks, antiquarks, and gluons [22].

Very strong limits on heavy isotope abundance in turn require the gluino to decay on Gyr time scales [23], leading to an upper bound for the scale of SUSY breaking $\mathcal{O}(10^{13})$ GeV. More restrictive bounds on Λ_{SUSY} can be determined from cosmological considerations [24]. Specifically, gluino decays would disturb predictions of big bang nucleosynthesis (BBN), distort the cosmic microwave background (CMB), or alter the diffuse gamma ray background. The details depend on both $M_{\tilde{g}}$ and $\tau_{\tilde{g}}$. For example, for $1 \lesssim M_{\tilde{g}}/\mathrm{TeV} \lesssim 5$, to avoid altering the abundances of D and ^{6}Li, $\tau_{\tilde{g}} \lesssim 100$ s, implying $\Lambda_{\mathrm{SUSY}} \lesssim 10^{10}$ GeV [24]. The relic abundance of lighter gluinos, $M_{\tilde{g}} \lesssim 500$ GeV, is constrained by COBE [25], WMAP [26], and EGRET observations [27]. On the one hand, gluinos that decay during or after the thermalization epoch can distort the CMB spectrum [28] and so are limited by COBE/WMAP observations. On the other hand, gluinos that decay after the recombination epoch give rise to pions which subsequently decay into γ rays that free-stream to us. The contribution of such a decay chain to the diffuse γ-ray background [29] is limited by EGRET observations.

Long-lived gluinos are also constrained by collider searches. Charged R-hadrons can be observed as they cross the detector either by their time delay relative to ultrarelativistic particles [30], or by their anomalously high ionization energy loss [31]. Besides, the energy deposition of neutral R-hadrons in the calorimeter is rather soft, and so when they are produced in association with a high-p_T jet they can be observed in the monojet channel + missing energy $\not{E}_T$: CDF run I data [32] found a bound of $M_{\tilde{g}} > 170$ GeV [16]. In addition, R-hadrons can become stopped gluinos by losing all of their momentum and coming to rest in the calorimeter [17]. The D0 Collaboration [33] has recently searched for stopped gluinos decaying into a single jet and a neutralino. The non-

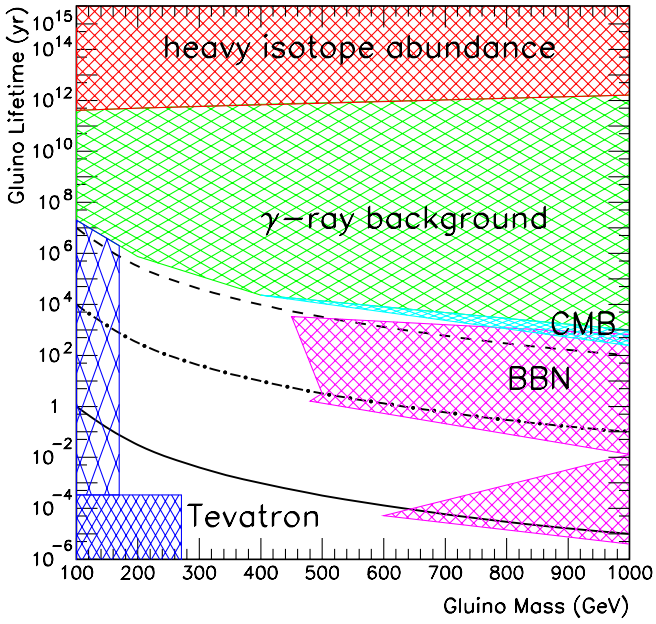

FIG. 1 (color online). Limits on long-lived gluinos. The cross-hatched bands indicate excluded regions of the $M_{\tilde{g}}$-$\tau_{\tilde{g}}$ plane from anomalous heavy isotope abundance [23], CMB [25] and EGRET [27] observations, BBN predictions [24], and collider data [16,33]. Contours of constant values of Λ_{SUSY} are also shown by solid (10^{10} GeV), dash-dotted (10^{11} GeV), and dashed lines (10^{12} GeV).

observation of monojets (above the expected background from cosmic-muon induced showers) in run II data implies $M_{\tilde{g}} > 270$ GeV for $\tau_{\tilde{g}} < 3$ hr All these limits are shown in Fig. 1. As we will show here, the study of hadronized gluinos originating in distant astrophysical sources provides a viable experimental handle in the region $300 \lesssim M_{\tilde{g}}/\mathrm{GeV} \lesssim 500$–$10^2 \lesssim \tau_{\tilde{g}}/\mathrm{yr} \lesssim 10^5$, which is yet unexplored.

The main goal of this paper is to describe a full-blown Monte Carlo simulation of R air showers, and uncover observables which may be exploited by new experiments like at the Pierre Auger Observatory [34]. This analysis expands on previous work [35] by including all possible R interactions and analyzing in detail the potential of the surface array. Before describing the simulation, we introduce in the following section the main properties of R-hadron interactions.

II. COSMIC R's

The origin cosmic rays is still an open question, with the degree of uncertainty increasing with rising energy [36]. Theoretically, one expects the cosmic ray spectrum to fall off somewhat above $10^{10.7}$ GeV, because the particle's energy gets degraded through interactions with the cosmic microwave (protons and nuclei) and radio (photons) backgrounds, a phenomenon known as the Greisen-Zatsepin-Kuzmin (GZK) cutoff [37]. The most recent data from the

Pierre Auger Observatory in fact do not indicate (yet) any excess beyond the expected cutoff [38]. Because of the rapid energy degradation, the maximum attainable energy in far away sources can be considerably higher than the GZK threshold. However, measurements of the GeV diffuse gamma ray flux significantly constrain the cosmic ray production integrated over redshift, and consequently limit the maximum energy of these particles. Specifically, the intermediate state of the reaction $p\gamma_{\rm CMB} \to N\pi$ is dominated by the Δ^+ resonance (because the neutron decay length is smaller than the nucleon mean free path on the relic photons). Hence, there is roughly an equal number of π^+ and π^0. Gamma rays, produced via π^0 decay, subsequently cascade electromagnetically on the cosmic radiation fields through e^+e^- production followed by inverse Compton scattering. The net result is a pileup of gamma rays at GeV energies, just below the threshold for further pair production. Therefore, if the distribution of cosmic ray sources is homogeneous and each source is characterized by a hard injection spectrum $\propto E^{-1}$, then EGRET measurements in the 100 MeV–100 GeV region [27] limit the maximum proton energy $\sim 10^{13.5}$ GeV [39]. Since Fermi's acceleration mechanism predicts a rather steeper spectrum $\propto E^{-2}$ [36], one can assume a maximum proton energy $E^{\rm lab}_{p,\rm max} \sim 10^{13.7}$ GeV.

Gluinos are flavor singlets of a color $SU(3)$ octet that interact strongly with the octet of gluons and can combine with quarks, antiquarks, and gluons to form colorless hadrons [22]. The bosonic states, $\tilde{g}qqq$, are generically called R-baryons, whereas the fermionic states, $\tilde{g}q\bar{q}$ and $\tilde{g}g$, are called R-mesons and R-glueballs, respectively. Very little is certain about the spectroscopy of these strongly interacting particles. The most relevant feature is (perhaps) the difference in mass between R-mesons (-glueballs) and R-baryons, because if $M_{R_{m(g)}} + m_N > M_{R_b} + m_\pi$, then there are exothermic conversions of $R_{m(g)}$ into R_b as the R-hadrons propagate in the atmosphere.

R-hadron states should be produced in pairs through pp collisions at powerful cosmic ray engines (e.g., protons undergoing acceleration in compact jets of relativistic plasma interact with those in the surrounding gas). The average energy of the produced R in the target system is

$$E_R^{\rm lab} \simeq \sqrt{\frac{E_p^{\rm lab}}{2m_p}} E_R^{\rm cm}, \tag{2}$$

where $E_p^{\rm lab}$ is the energy of the proton undergoing acceleration at the source, $E_R^{\rm cm} \simeq \sqrt{\hat{s}}/2$ is the average R-energy in the center of mass (c.m.) of the pp collision, and $\hat{s}$ is the square of the energy in the c.m. of the parton-parton collision. Now, by restricting R-production to large c.m. energies (say, $\hat{s} \geq 16M_R^2$), from Eq. (2) we obtain the maximum energy of cosmic R's, $E_R^{\rm lab} < 10^7 M_R$. Thus, the R-spectrum cuts off at lower energy than the cosmic ray spectrum. Since these particles originate from cosmological distance d, to reach the Earth the gluinos must be remarkably long lived, $\tau_{\tilde{g}} \gtrsim 100(M_{\tilde{g}}/500\ {\rm GeV}) \times (d/{\rm Gpc})$ yr. Moreover, to avoid deflections on the extragalactic magnetic fields and the consequent energy loss due to pair production and other mechanisms (such as synchrotron or bremsstrahlung radiation), the R-hadron has to be neutral [40]. The overall intensity of R-hadrons is constrained by its accompanying pion flux, which decays into γ rays and neutrinos that can be confronted with existing data [27,41]. Unfortunately, the expected flux of ultrarelativistic (Lorentz factors $\sim 10^7$) R-hadrons is found to be very low (less than 6 particles per km^2 per millennium [20]), and so the only experimental method with potential is observation of their interactions in large volumes of the Earth's atmosphere.

When a hadronized gluino impinges on a stationary nucleon of the Earth's atmosphere, a large number (over 140 when summed over all R-hadrons) of scattering processes are possible [42]. Interactions of R-meson states include (i) $2 \to 2$ processes, such as purely elastic (e.g. $\tilde{g}d\bar{d} + uud \to \tilde{g}d\bar{d} + uud$), charge exchange (e.g. $\tilde{g}d\bar{d} + uud \to \tilde{g}u\bar{d} + udd$), and baryon exchange (e.g. $\tilde{g}d\bar{d} + uud \to \tilde{g}udd + u\bar{d}$); and (ii) $2 \to X$ processes including normal inelastic scattering (e.g. $\tilde{g}d\bar{d} + uud \to \tilde{g}u\bar{d} + udd + d\bar{d}$) and inelastic scattering with baryon exchange (e.g. $\tilde{g}d\bar{d} + uud \to \tilde{g}uud + u\bar{d} + d\bar{u} + d\bar{d}$). Since the final-state pion is so light, processes with baryon exchange would be kinematically favored. However, these processes could be dynamically suppressed because the exchange of two quarks is required. Interactions of R-baryon states include purely elastic, charged exchange, and normal inelastic scattering. No baryon exchange is possible because of the negligible probability for a $\tilde{g}qqq$ to interact with a pion in the nucleus. Furthermore, this process would be kinematically strongly disfavored. Consequently, R-mesons can convert into R-baryons, but not vice versa. Interactions of R-glueballs are expected to be similar to those of R-mesons. This is because a g is able to split into a $q\bar{q}$ state, suggesting that a $\tilde{g}g$ interacts like (and mixes with) $\tilde{g}q\bar{q}$ states.

To establish which of these processes dominates, aside from a model describing the target (neutron or proton), the relative couplings of all the processes must be known. The latter requires the calculation of the Clebsch-Gordan coefficients of isospin-related processes, and the evaluation of all additional dynamical effects for all processes. To parametrize our ignorance about QCD interactions, here we will consider all the relevant processes mentioned above (5 for R-mesons, and 3 for R-baryons), assigning them different probabilities *ad hoc* so as to explore the entire parameter space.

Predicting the total cross section of an R-hadron scattering off a nucleon is nontrivial. However, because of the high c.m. energies under consideration in this paper, the

cross section can be safely approximated by the geometrical cross section. Moreover, since the size of the R-hadron is roughly the same as the size of the accompanying hadron system, the total cross section for nucleon scattering can be approximated by the asymptotic values for the cross sections for normal hadron scattering off nucleons. Therefore, for R-baryons we take $\sigma_{R_b-p}(\sqrt{s} \simeq 10^5 \text{ GeV}) \approx 140$ mb [43]. This corresponds to a cross section for scattering off air molecules $\sigma_{R_b-\text{air}}(\sqrt{s} \simeq 10^5)$ GeV ≈ 520 mb, yielding a mean free path in the atmosphere, $\lambda_{R_b} = m_{\text{air}}/\sigma_{R_b-\text{air}} \approx 47$ g/cm^2, where we have taken $m_{\text{air}} \approx 2.43 \times 10^{-23}$ g (corresponding to an atomic mixture of 78% N, 21.05% O, 0.47% Ar, and 0.03% of other elements). At this c.m. energy, the π-air cross section is roughly 90% of the p-air cross section [44]; hence for R-meson states we set $\lambda_{R_m} = 52$ g/cm^2. R-glueballs are expected to have the same cross section as R-mesons. This is because the geometrical cross section is approximated by the high energy hadron cross section, where gluon exchange dominates [the gg coupling is a factor $9/4$ larger than the qg coupling, but a meson has 2 quarks, resulting in a cross section of a $\tilde{g}g$ state which is $(9/4)/(1+1) \simeq 1$ times the cross section for a $\tilde{g}q\bar{q}$ state]. With this in mind we set $\lambda_{R_m} \simeq \lambda_{R_g}$.

In analogy to a billiard ball moving through a sea of ping-pong balls, the R suffers very little energy loss as it traverses the atmosphere. Then, for R-flippers (i.e., $R_{m(g)} \rightarrow R_b$) we assume that the emitted pion has an energy $E_\pi \approx \Gamma m_\pi$, where Γ is the Lorentz factor of the incoming R-hadron. This means that most of the energy $\sim \Gamma M_{\tilde{g}}$ is carried by the accompanying R_b produced in the interaction. Following [20], for inelastic collisions we parametrize the fractional energy loss per collision as $K_{\text{inel}} \approx (M_R/\text{GeV})^{-1}$. For completeness, a derivation of this relation is given in the Appendix.

III. THE PIERRE AUGER OBSERVATORY

The Pierre Auger Observatory (or simply "Auger") [34] is designed to study cosmic rays with energies above about 10^9 GeV, with the aim of uncovering their origins and nature. Such events are too rare to be directly detected, but the direction, energy, and to some extent the chemical composition of the primary particle can be inferred from the cascade of secondary particles induced when the primary particle impinges on the upper atmosphere. These cascades, or air showers, have been studied by measuring the nitrogen fluorescence they produce in the atmosphere or by directly sampling shower particles at ground level. Auger is a hybrid detector, exploiting both of these well-established techniques, by employing an array of water Čerenkov detectors overlooked by fluorescence telescopes. On clear moonless nights, air showers are simultaneously observed by both types of detectors, facilitating powerful reconstruction methods and control of the systematic errors which have plagued cosmic ray experiments to date.

The observatory is now operational on an elevated plane in western Argentina and is in the process of growing to its final size of 3000 km^2. The surface detector (SD) consists of an array of 1600 water tanks deployed on a hexagonal grid with spacing of 1.5 km. These tanks detect the Čerenkov light produced by shower particles crossing their 1.2 m $\times$ 10 m^2 water volume, thanks to three 9-inch photomultipliers. The fluorescence detector (FD) consists of four ensembles of six telescopes, each of which has a field of view of 30° vertically and 30° horizontally (i.e., 180° for each fluorescence detector site). The geography of the northern site would accommodate a larger array (of up to 10 370 km^2 [45]), allowing higher sensitivity to the low flux of cosmic R's.

Identifying showers themselves is usually straightforward, as there is essentially no "background" for the detectors, at least above their energy threshold. In the case of Auger, the threshold for the surface detector is around $10^{8.6}$ GeV, below which less than 10% of the showers can trigger three tanks or more, as required. However, full detection efficiency (i.e., 100% or "saturated acceptance") is achieved only around $10^{9.5}$ GeV for showers with a zenith angle lower than 60°, and lower energy showers are usually discarded to avoid any complication caused by the energy dependence of both the detection efficiency and the energy resolution. For fluorescence detectors, showers with energies as low 10^8 GeV can be observed. However, the corresponding acceptance is relatively low, since the total intensity of the fluorescence light does not allow detection from a large distance, and the shower maximum is then usually above the field of view of the telescopes, which prevents accurate reconstruction. Like for any fluorescence detector, the acceptance of the eyes of Auger increases with energy (as bigger showers can be seen from larger distances) and depends on the atmospheric conditions. However, a precise determination of the fluorescence detector acceptance is not crucial; thanks to its hybrid nature, the energy differential flux (or "spectrum") is not obtained from the fluorescence detector, but from the surface detector whose absolute acceptance is essentially geometrical above saturation and thus is controlled within a few percent at most.

Identifying the primary particle species is somewhat more difficult as one has to search for differences in the shower development, which are usually relatively small and subject to fluctuations associated with the stochasticity of the first interactions [46]. However, as we discuss in the next sections the showers initiated by R-hadrons have very distinctive characteristics and can be easily isolated from background.

IV. AIR SHOWER SIMULATIONS

The AIRES simulation engine [47] provides full space-time particle propagation in a realistic environment, taking into account the characteristics of the atmospheric density

profile (using the standard U.S. atmosphere [48]), the Earth's curvature, and the geomagnetic field (calculated for the location of Auger with an uncertainty of a few percent [49]).

The following particles are taken into account in the AIRES simulations: photons, electrons, positrons, muons, pions, kaons, eta mesons, lambda baryons, nucleons, antinucleons, and nuclei up to $Z = 36$. Nucleus-nucleus, hadron-nucleus, and photon-nucleus inelastic collisions with significant cross sections are taken into account in the simulation. The hadronic processes are simulated using different models, accordingly to the energy: high energy collisions are processed invoking an external package (SIBYLL 2.1 [50] or QGSJET II [51]), while low energy ones are processed using an extension of the Hillas splitting algorithm (EHSA) [52]. The threshold energies separating the low and high energy regimes used in our simulations are 200 GeV and 80 GeV for the SIBYLL and QGSJET, respectively. The EHSA low energy hadronic model used in AIRES is a very fast procedure, effectively emulating the major characteristics of low energy hadronic collisions. The model is adjusted to retrieve similar results as the high energy hadronic model for energies near the transition thresholds previously mentioned, and the low energy cross sections are calculated from parametrizations of experimental data. A complete discussion on the low energy hadronic models is clearly beyond the scope of this paper. A separate report on this subject will be published elsewhere [53].

The AIRES program consists of various interacting procedures that operate on a data set with a variable number of records. Several data arrays (or stacks) are defined. Every record within any of these stacks is a particle entry and represents a physical particle. The data contained in every record are related to the characteristics of the corresponding particle. The particles can move inside a volume within the atmosphere where the shower takes place. This volume is limited by the ground, the injection surfaces, and by vertical planes which limit the region of interest. Before starting the simulation, all the stacks are empty. The first action is to add the first stack entry, which corresponds to the primary particle. Then the stack processing loop begins. The primary particle is initially located at the injection surface, and its downward direction of motion defines the shower axis. After the primary particle's fate has been decided, the corresponding interaction begins to be processed. The latter generally involves the creation of new particles which are stored in the empty stacks and remain waiting to be processed. Particle entries are removed when one of the following events happens: (a) the energy of the particle is below the selected cut energy; (b) the particle reaches ground level; (c) a particle going upwards reaches the injection surface; (d) a particle with quasihorizontal motion exits the region of interest. After having scanned all the stacks, it is checked whether or not there are new particle entries pending further processing. If the answer is positive, then all the stacks are scanned once more; otherwise the simulation of the shower is complete.

AIRES has been successfully used to study several characteristics of high energy showers, including comparisons between hadronic models [54], influence of the Landau-Pomeranchuk-Migdal effect [55], muon bremsstrahlung [56], and geomagnetic deflections [49] on the shower development. AIRES has also been successfully used to determine the efficiency of Auger for quasihorizontal showers generated by τ neutrinos [57], to estimate the flux of atmospheric muons [58], and to study the production of black holes in TeV-scale gravity models [59]. For the present analysis, we prepared a new module to account for the simulation of cosmic R's. The module includes external parameters such as the type of primary hadron (R_b or R_m), its mass M_R, its charge, and its primary energy $E_R^{\rm lab}$. We adopt the atmospheric mean free path derived in the previous section.

The total interaction probability is managed by five parameters (P_i, $i = 1, \ldots, 5$) which measure the weights of the different processes. (1) The parameter P_1 measures the probability of an elastic scattering. The program emulates this process by transferring a small part of the R-energy (~ 1 TeV) to an air nucleus which is injected into the shower. (2) The parameter P_2 measures the probability of an elastic scattering with charge exchange, in which there is again a small transfer of energy to an air nucleus, but now the R primary also flips its charge. (3) The parameter P_3 accounts for baryon exchange. In this case, a pion with energy $E_\pi = m_\pi(\overline{E_R^{\rm lab}}/M_R)$ is injected into the shower evolution, where $\overline{E_R^{\rm lab}}$ is the energy of the R-hadron before the collision. If the incoming R-hadron is neutral, then the outgoing pion is charged and vice versa. The R-hadron mutates into a baryon with $\widetilde{E_R^{\rm lab}} = \overline{E_R^{\rm lab}} - E_\pi$. (4) In the inelastic process, controlled by P_4, the R-hadron transfers an energy $E_{\rm coll} = \overline{E_R^{\rm lab}} K_{\rm inel}$ to the shower. The process is simulated with the help of the standard packages of AIRES for nucleon and pion collisions. A neutron (of energy $E_{\rm coll}$) scatters off an air nucleus if the primary is an R_b^0, and a proton if it is an $R_b^\pm$. If it is an R_m^0 the projectile particle (simulating the R collision) is a π^0, whereas if it is an $R_m^\pm$ the projectile is a $\pi^\pm$. All the secondaries resulting from this interaction are considered in the subsequent shower evolution. Finally, (5) P_5 controls the inelastic scattering with baryon exchange. It is simulated as a combination of processes (3) and (4), i.e., the emission of a pion followed by an inelastic collision. In our simulations we take $P_5^m = 0.8 - P_4^m$, with $0 < P_4^m < 0.8$.

For the simulation engine, the shower starts when the R-hadron is added to the previously empty stack. The injection surface is located at the top of the atmosphere, spacing the interaction point according to an exponential distribution with mean equal to $\lambda_{R_{\rm b(m)}}$. The interaction

TABLE I. Interaction probabilities for the possible R-hadron scattering processes.

Hadron	P_1	P_2	P_3	P_4	P_5
R_b	0.1	0.1	0	0.8	0
R_m	0.05	0.05	0.1	P_4^m	P_5^m

probabilities P_i are given in Table I. The R-hadron is tracked until it reaches ground level or else its energy is degraded below 100 MeV. New stack entries are appended to the existing lists for every SM particle produced in the R-interactions. These entries are then repeatedly processed sequentially by means of the algorithms implemented in AIRES.

As an illustration, we have run a set of air shower simulations, with $M_R = 500$ GeV and $E_R^{\rm lab} = 10^{9.7}$ GeV [60]. In Fig. 2 we show the energy fraction dissipated into "visible" particles in R-hadron air showers, as predicted by our simulations. One can see from the figure that there needs to be sufficient path length for the R, with its low inelasticity, to lose sufficient energy. The experimentally interesting region to search for R-hadrons is then $70° \lesssim \Theta \lesssim 90°$.

Because of the very low inelasticity of R-air interactions, the leading particle retains most of its energy all the way to the ground, while the secondary particles promptly cascade to low energies as for any other air shower. This results in an ensemble of mini-showers strung along the trajectory of the leading particle. Since the typical distance between mini-showers is about 10 times smaller than the extent of a single longitudinal profile, it is not possible to resolve the individual showers experimentally. Instead, one observes a smooth envelope encompassing all the mini-showers, which extends from the first interaction all the way to the ground; see Fig. 1 in Ref. [35]. The R-hadron air showers then present a distinct profile: the flatness of the longitudinal development is unique to the extremely low inelasticity of the scattering, and can be easily isolated from the background. However, it turns out that there is a sharp cutoff in the production of cosmic R's at $E_R^{\rm lab} \approx 10^{9.5}$ GeV [20], which unfortunately leads to showers below detection threshold for the fluorescence method (except for a very small aperture comprised of regions close to the telescope).

In Fig. 3 we show a comparison of the total signal at ground level for R and proton air showers. To compute the total signal of a single shower, we first consider all particles reaching the ground with a distance to the shower axis $r > r_0$, with r_0 conveniently chosen to be 250 m, and for each particle we simulate the Čerenkov detector response. The total signal of a given shower, $S(r > r_0)$, is the sum of each particle's individual signal normalized to 1 for proton showers of 10^{10} GeV and incident zenith angle of 60°. It is clear that the total R signal at ground level increases with zenith angle, because of the larger slant depth. This is in sharp contrast to proton showers, in which the signal is reduced with increasing Θ because of the greater shower age.

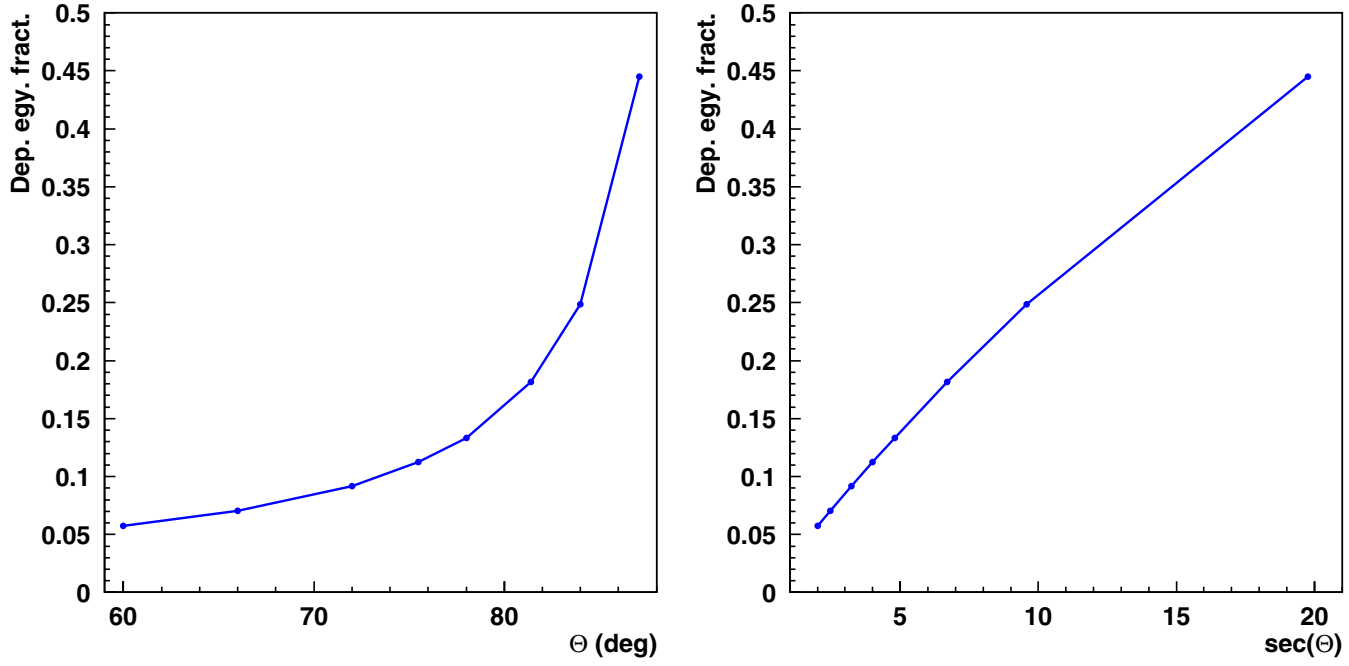

FIG. 2 (color online). Energy fraction deposited in the atmosphere during R-hadron air showers as a function of the zenith angle Θ (left panel) and secΘ (right panel). The curves represent an average over the different species. We note that the distinguishing power among the various species is very limited for the entire range of P_4^m.

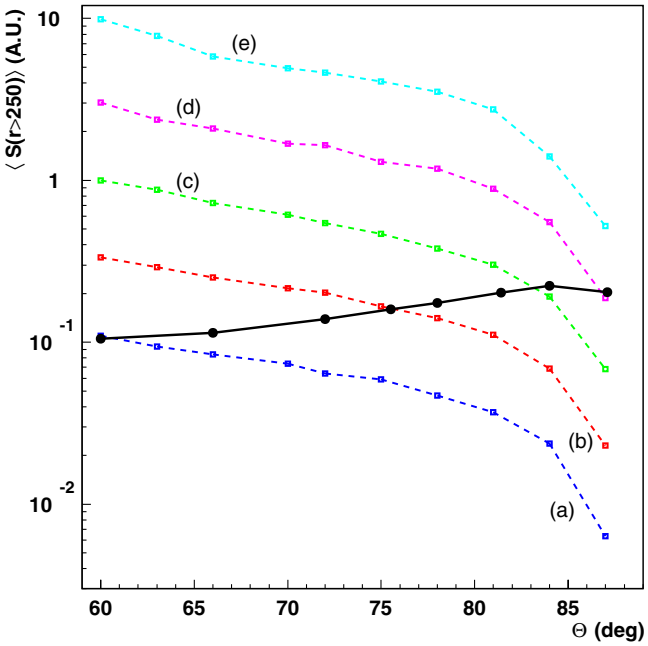

FIG. 3 (color online). Average total signal beyond 250 m from the shower core versus shower zenith angle. Signals are normalized to 1 for the case of 10^{10} GeV proton showers inclined 60°. The dashed lines correspond to proton showers of primary energy: (a) $10^{9.0}$ GeV, (b) $10^{9.5}$ GeV, (c) $10^{10.0}$ GeV, (d) $10^{10.5}$ GeV, (e) $10^{11.0}$ GeV. The solid line corresponds to R-hadron showers. The lines are only to guide the eye.

As discuss in Sec. III, the relation between the signal observed at the surface detectors and the primary energy is determined using hybrid events in which the fluorescence eyes are thought to provide a reliable measurement of the total energy. For proton showers the surface detectors sample about 1% to 10% of the shower energy. Because of the electromagnetic component recycling, the R-hadron produces a somewhat larger signal at ground level than one would expect from standard baryonic showers. As one can check in Table II, for large zenith angles if one assumes the shower properties are the characteristics of proton showers then the total primary energy would be overestimated. Note that this aspect is not compensated by the calibration procedure, because the R-component does not deposit significant energy in the region of the atmosphere used in the fluorescence-based calibration. In summary, although the total contribution to the shower energy is small, the R-hadron deposits a disproportionally large fraction of their energy close to the ground. Consequently, cosmic R's would induce a significant signal in the surface array but not in the fluorescence eyes. In what follows we use these shower characteristics to construct observables which may be used to distinguish the R-hadron from traditional cosmic ray showers.

TABLE II. Primary proton energy $E_p^{\rm lab}$ required to produce the same total signal at ground level as an R-hadron with $E_R^{\rm lab} = 10^{9.7}$ GeV, at different zenith angles.

Θ	60°	66°	72°	75.5°	78°	81.4°	84°	87.1°
$E_p^{\rm lab}$(GeV)	$10^{9.0}$	$10^{9.2}$	$10^{9.3}$	$10^{9.5}$	$10^{9.6}$	$10^{9.8}$	$10^{10.1}$	$10^{10.5}$

V. GROUND ARRAY SIGNAL

The surface detectors of the Auger Observatory are capable of measuring the signal associated with an incoming shower as a function of time. Since a high energy event triggers many detectors, placed at different distances from the shower axis, it is possible to reconstruct the lateral-time distribution of the signal $S(r, t)$. $S(r, t)dt$ gives the amount of signal at a (3-dimensional) distance r from the shower axis, produced at the time interval $[t, t + dt]$. For convenience, the origin of times is defined for each point in the ground surface as the instant when a plane orthogonal to the shower axis, synchronized with the primary particle and moving towards the ground at the speed of light, intersects the corresponding point. In this way, $S(r, t)$ is necessarily zero for negative times. With this definition, the time t is frequently called "arrival time delay."

The total signal at a given distance from the shower axis is the signal accumulated over all times, that is,

$$S_{\rm tot}(r) = \int_0^\infty S(r, t)dt. \tag{3}$$

Other quantities that are usually used in the analysis of SD signals are as follows:

(i) Shower front arrival time, t_0 ($t_0 \geq 0$). This is the time corresponding to the first nonzero shower signal at the given point. t_0 is directly related to the shower front curvature.

(ii) Partial rise times, t_x, defined as the time elapsed until the accumulated signal is a fraction x of the total signal, that is,

$$\int_0^{t_x} S(r, t)dt = xS_{\rm tot}(r). \tag{4}$$

Common values of x are 10%, 50%, and 90%. t_x is a growing function of r, especially far from the shower axis.

The lateral-time distribution of the signal is a SD observable capable of characterizing showers initiated by cosmic rays. Consider, for example, a typical shower initiated by a vertical proton. In Fig. 4 the corresponding lateral-time signal distribution is displayed using a false color (or gray scale) diagram. From this figure it is possible to notice the main features of such a distribution: (i) most of the shower particles arrive near the shower axis, that is, the *signal lateral distribution* $S_{\rm tot}(r)$ decreases with r; (ii) $t_0(r)$ increases with r, as expected, because particles must travel longer distances and undergo more interactions to reach positions located far from the shower axis; (iii) the time interval of the signal at a given point grows with r. In

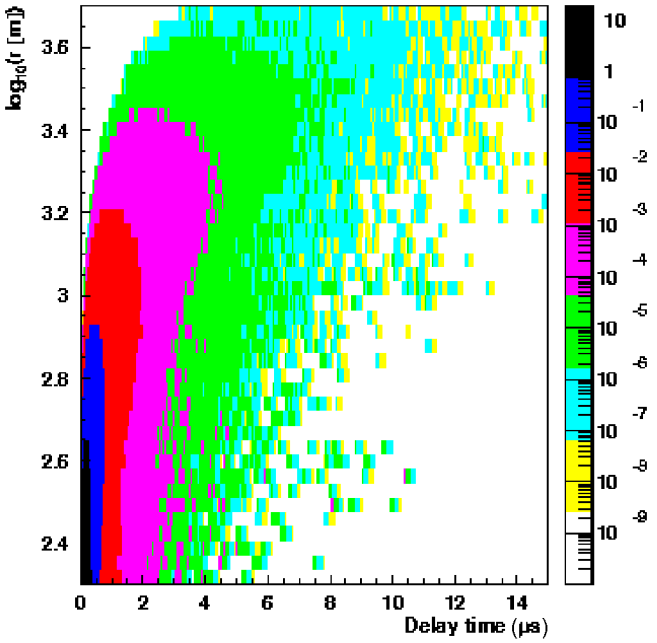

FIG. 4 (color online). Lateral versus arrival time delay distribution for a vertical shower initiated by a $10^{9.5}$ GeV proton.

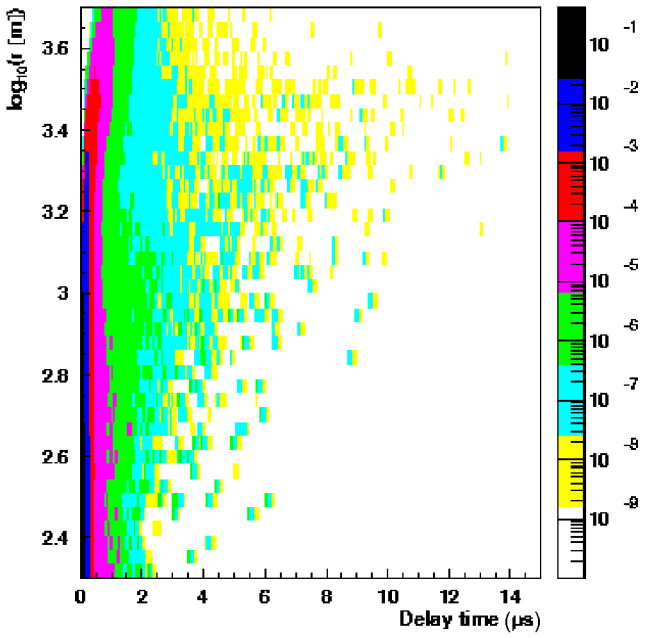

FIG. 5 (color online). Same as Fig. 4 but in the case of $10^{9.5}$ GeV protons inclined 75 degrees.

the example of Fig. 4 it goes from some 4 μs at $r = 300$ m to about 12 μs for $r > 3000$ m.

If the inclination of a shower is increased, the thickness of the air layer placed between the point where the cosmic particle enters the atmosphere and ground level also increases. As a result, the age of the detected shower increases too. In the case of showers initiated by hadronic primaries like protons and nuclei, the aging of inclined showers at ground level becomes evident for inclinations larger than 65 degrees, because of the practically complete attenuation of the electromagnetic component of the shower. For such inclinations, the muonic component becomes very important (see Fig. 2 of Ref. [49]), because it produces significant modifications in the detected signal. In particular, the shower front becomes flatter, and the signal is concentrated within a relatively small time span. These characteristics show up clearly in Fig. 5, where $S(r, t)$ is plotted for showers initiated by protons with the same energy as the showers shown in Fig. 4, but for an inclination of 75 degrees with respect to the vertical.

The lateral-time signal distributions of inclined showers initiated by R-hadrons present a substantially different aspect, when compared with the proton case. In Fig. 6 the signal distribution corresponding to $10^{9.7}$ GeV R-hadron showers inclined 75 degrees is displayed. A comparison with the distribution of Fig. 5 leads to the following conclusions: (i) the R-hadron distribution is slightly more concentrated near the shower axis, and (ii) the time span of the signal is substantially larger than in the proton case (note that the primary energy of the proton showers has been chosen accordingly with Table II such that the amount of signal for $r > r_0$ is, on average, the same for both primaries).

The last feature of the lateral-time distribution of R-hadron showers is certainly the most clear signature of such events that could be found in our simulation study. Combined, in the case of hybrid events, with a neatly different longitudinal development, and inconsistent en-

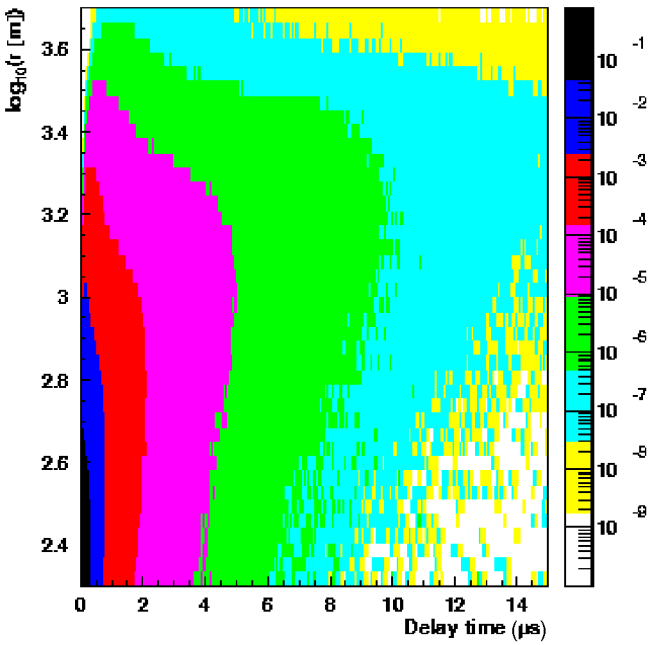

FIG. 6 (color online). Same as Fig. 4 but for showers initiated by $10^{9.7}$ GeV R-hadrons inclined 75 degrees.

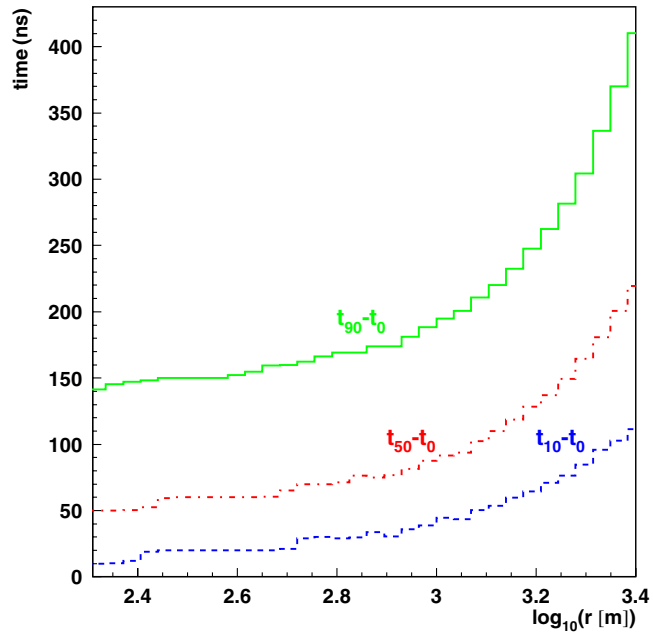

FIG. 7 (color online). t_{10}-t_0, t_{50}-t_0, and t_{90}-t_0 plotted versus the logarithm of the distance to the shower axis. The data correspond to $10^{9.5}$ GeV protons inclined 75 degrees.

ergy measurements, *R*-hadron events can be clearly distinguished from hadronic ones, and also from neutrino initiated showers where the FD energy determination will be very different from the present case of *R*-hadron showers.

The different time span of signals can be quantified more precisely studying the observables t_{10}, t_{50}, and t_{90}. Figures 7 and 8 contain plots of these observables as

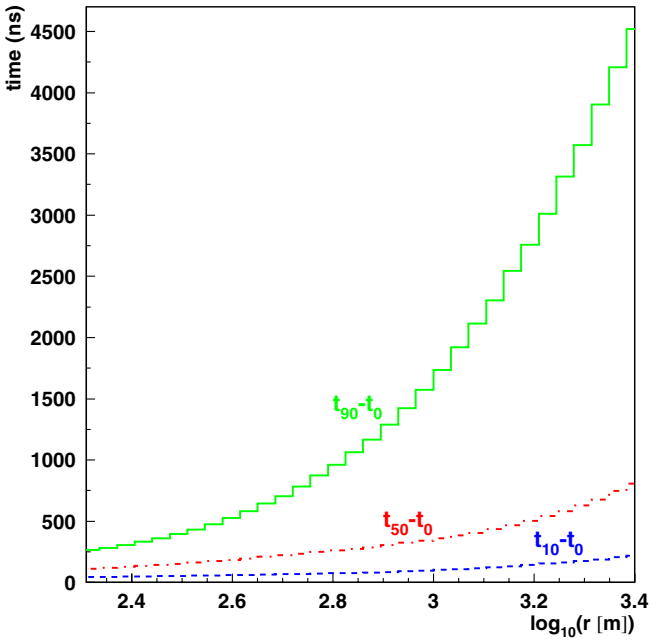

FIG. 8 (color online). Same as Fig. 7, but for $10^{9.7}$ GeV *R*-hadrons inclined 75 degrees.

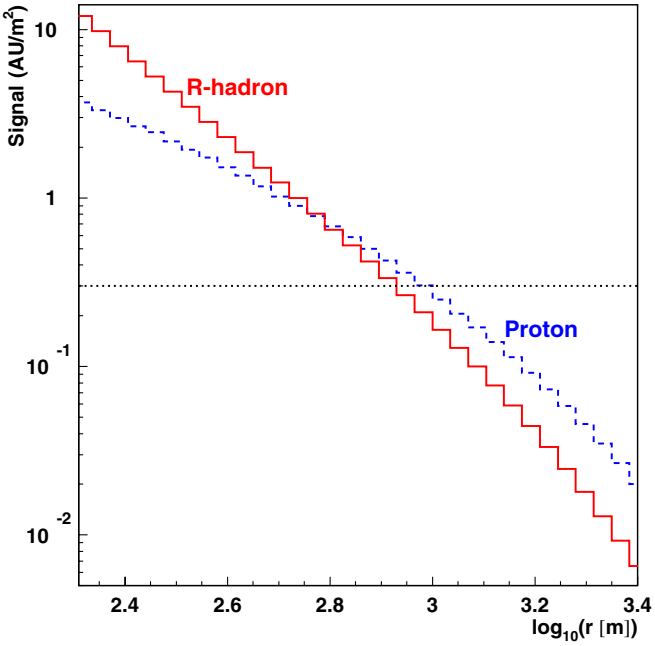

FIG. 9 (color online). Water Čerenkov signal plotted versus the logarithm of the distance to the shower axis. The solid (dashed) histogram correspond to *R*-hadron (proton) primaries. The horizontal dotted line indicates (approximately) the threshold of Auger surface detectors.

functions of $\log_{10}(r)$, in the case of proton and *R*-hadron showers, respectively. The larger time span of the signals in the *R*-hadron case is evident for all the plotted quantities (note the different time scales used in either figure).

The total signal as a function of the distance to the shower axis, $S_{\rm tot}(r)$, called *lateral distribution*, is another fundamental observable that can be measured with the Auger surface detectors. It is the most important observable for SD energy determination in the case of showers with an inclination of less than 65 degrees.

We have studied the behavior of the lateral distribution in the case of *R*-hadrons, comparing the results with the corresponding ones for showers initiated with protons. The results, displayed in Fig. 9, clearly show that the signal corresponding to *R*-hadron showers is more concentrated near the shower axis. This also implies a different slope for the distributions that could eventually be measured. As a reference, a qualitative indicator of the signal threshold of Auger detectors is also shown in the figure (dotted line).

VI. CONCLUSIONS

In this paper we have analyzed the characteristics of air showers produced by gluino-containing hadrons. Using AIRES, we have performed a high statistics set of full quality showers initiated by *R*-hadrons. We have considered both *R*-baryon and *R*-meson primaries. The analysis of standard observables that can be measured by hybrid air shower experiments like Auger shows that atmospheric

cascades initiated by R-hadrons are significantly different from ''classical'' showers, such as, for example, those initiated by cosmic protons. Our study indicates that if cosmic R-hadrons do exist they would produce a particular signature that will be visible at Auger: at ground level, the R-hadron showers are characterized by the presence of a strong electromagnetic component at all zenith angles. This implies a much longer time span for the signal, in comparison with proton showers. At the same time, the mini-showers generated by the passage of the R-hadron across the atmosphere produce narrower lateral distributions than the corresponding ones for the proton case.

If R-hadron events are analyzed with the standard protocol for hadronic primary showers, a series of inconsistencies will be present. In particular, the energy determination via ground signal analysis of very inclined showers [61] will likely lead to a primary energy overestimation. On the other hand, an eventual hybrid event of this kind will show a limited, or even below threshold FD signal. This leads to contradictory FD and SD energy determinations. Moreover, these ''golden'' events would allow identification of R-hadrons from eventual quasihorizontal neutrino events that are likely to generate showers with similar ground signal, but non-negligible fluorescence contribution [62].

The pertinent question at this point is whether existing experiments have already collected events exhibiting the characteristics of gluino showers described above. None of the ultrahigh energy cosmic ray experiments have thus reported such results. It is interesting to note, however, that the 10^6 GeV ''Centauro'' events detected at Mt. Chacaltaya [63] might be suggestive of gluino-induced showers. In these events, the ratio of hadronic to electromagnetic components is about 50:1, contrary to the expectation of dominance of the electromagnetic component in vertical baryon-induced showers. The most carefully considered explanation to date is the explosive quark matter model [64]. Interestingly, though, heavy high energy gluinos could also produce such an inverted hadronic electromagnetic ratio. This is because the multiple low-inelasticity collisions would result in hadronic superimposed showers. At the detector level (~ 5200 m), the electromagnetic component of the subshowers would be mostly filtered out, while the superposed hadronic showers would survive. This is because the ''low'' energy (~ 100 TeV) electromagnetic subshowers induced by high energy R-hadrons would develop faster (being quickly quenched by atmospheric losses) than the high energy ($\sim 10^6$ GeV) electromagnetic subshowers induced by ultrahigh energy R-hadrons. It is also interesting to note that this explanation of the Centauro events does not predict any phenomenon one might observe at a collider experiment, consistent with the null results from UA1 [64], UA5 [65], and CDF [66]. If, in fact, gluinos are guilty of producing the Centauro events, this would constitute the first evidence of a finely tuned universe from a cosmic ray observation.

ACKNOWLEDGMENTS

We would like to thank Haim Goldberg and Carlos Nuñez for discussions.

APPENDIX

Consider the process in which two particles of 4-momenta p_a and p_b and masses M_R and m_N scatter two particles of momenta p_c and p_d and masses M_R and M_X, respectively. Using the total 4-momentum P we define the vector

$$I_\alpha = \epsilon_{\alpha\beta\mu\nu} P^\beta p_a^\mu p_c^\nu \tag{A1}$$

and write the Lorentz-invariant form

$$I_\alpha I^\alpha = st(2M_R^2 + m_N^2 + M_X^2 - s - t) - t(M_R^2 - m_N^2)(M_R^2 - M_X^2) - M_R^2(M_X^2 - m_N^2)^2 \tag{A2}$$

in terms of the Mandelstam variables $s = (p_a + p_b)^2 = (p_c + p_d)^2$ and $t = (p_a - p_c)^2 = (p_b - p_d)^2$. Note that this squared invariant when viewed from the c.m. frame reduces to

$$\vec{I}^{*2} = \sqrt{s}(\vec{p}_a^* \times \vec{p}_c^*) = \sqrt{s}|\vec{p}_a^*||\vec{p}_c^*| \sin\theta^*, \tag{A3}$$

where θ^* is the scattered angle. Consequently, the forward direction is defined through the condition $I_\alpha I^\alpha = 0$. In the large s limit where

$$st(2M_R^2 + m_N^2 + M_X^2 - s - t) \approx -s^2 t, \tag{A4}$$

the minimum momentum transferred can be easily obtained by setting Eq. (A2) $= 0$ and solving for $t_{\min}$. All in all,

$$t_{\min} = -\frac{M_R^2(M_X^2 - m_N^2)^2}{(M_X^2 - M_R^2)(m_N^2 - M_R^2) + s^2} \approx -\frac{M_R^2 M_X^4}{s^2}. \tag{A5}$$

In the c.m. frame, $E_a^* = (s + M_R^2 - m_N^2)/(2\sqrt{s})$ and $E_c^* = (s + M_R^2 - M_X^2)/(2\sqrt{s})$ [2]. Therefore, the invariant quantity $(E_c - E_a)/E_a$ that describes the inelasticity of the process reads

$$K_{\text{inel}} \approx \frac{(s + M_R^2 - M_X^2) - (s + M_R^2)}{(s + M_R^2)} \approx -\frac{M_X^2}{s}. \tag{A6}$$

Now, combining Eqs. (A5) and (A6) we obtain

$$K_{\text{inel}} \approx \frac{|t_{\min}|^{1/2}}{M_R}. \tag{A7}$$

The QCD cross section falls off very rapidly and gets negligible for $t > \Lambda_{\text{QCD}}$. Thus, taking $\Lambda_{\text{QCD}} \approx 1$ GeV, Eq. (A7) leads to $K_{\text{inel}} \approx (M_R/\text{GeV})^{-1}$.

[1] S. Dimopoulos and H. Georgi, Nucl. Phys. **B193**, 150 (1981).

[2] S. Eidelman *et al.* (Particle Data Group Collaboration), Phys. Lett. B **592**, 1 (2004).

[3] N. A. Bahcall, J. P. Ostriker, S. Perlmutter, and P. J. Steinhardt, Science **284**, 1481 (1999).

[4] S. Weinberg, Phys. Rev. Lett. **59**, 2607 (1987).

[5] R. Bousso and J. Polchinski, J. High Energy Phys. 06 (2000) 006; A. Maloney, E. Silverstein, and A. Strominger, arXiv:hep-th/0205316; S. Kachru, R. Kallosh, A. Linde, and S. P. Trivedi, Phys. Rev. D **68**, 046005 (2003); L. Susskind, arXiv:hep-th/0302219; M. R. Douglas, J. High Energy Phys. 05 (2003) 046; S. B. Giddings, S. Kachru, and J. Polchinski, Phys. Rev. D **66**, 106006 (2002); S. Ashok and M. R. Douglas, J. High Energy Phys. 01 (2004) 060; F. Denef and M. R. Douglas, J. High Energy Phys. 05 (2004) 072; A. Giryavets, S. Kachru, and P. K. Tripathy, J. High Energy Phys. 08 (2004) 002; J. P. Conlon and F. Quevedo, J. High Energy Phys. 10 (2004) 039; O. DeWolfe, A. Giryavets, S. Kachru, and W. Taylor, J. High Energy Phys. 02 (2005) 037; K. R. Dienes, E. Dudas, and T. Gherghetta, Phys. Rev. D **72**, 026005 (2005).

[6] L. Susskind, arXiv:hep-th/0405189; M. R. Douglas, arXiv:hep-th/0405279. See also M. Dine, E. Gorbatov, and S. D. Thomas, arXiv:hep-th/0407043; E. Silverstein, arXiv:hep-th/0407202.

[7] H. Goldberg, Phys. Rev. Lett. **50**, 1419 (1983); J. R. Ellis, J. S. Hagelin, D. V. Nanopoulos, K. A. Olive, and M. Srednicki, Nucl. Phys. **B238**, 453 (1984).

[8] S. Dimopoulos, S. Raby, and F. Wilczek, Phys. Rev. D **24**, 1681 (1981).

[9] N. Arkani-Hamed and S. Dimopoulos, J. High Energy Phys. 06 (2005) 073.

[10] A. Delgado and G. F. Giudice, Phys. Lett. B **627**, 155 (2005); J. L. Feng and F. Wilczek, Phys. Lett. B **631**, 170 (2005); S. Weinberg, arXiv:hep-th/0511037.

[11] A. Arvanitaki, C. Davis, P. W. Graham, and J. G. Wacker, Phys. Rev. D **70**, 117703 (2004).

[12] G. F. Giudice and A. Romanino, Nucl. Phys. **B699**, 65 (2004); **B706**, 65(E) (2005).

[13] A. Pierce, Phys. Rev. D **70**, 075006 (2004); S. K. Gupta, P. Konar, and B. Mukhopadhyaya, Phys. Lett. B **606**, 384 (2005); R. Allahverdi, A. Jokinen, and A. Mazumdar, Phys. Rev. D **71**, 043505 (2005); A. Arvanitaki and P. W. Graham, Phys. Rev. D **72**, 055010 (2005); G. M. Vereshkov, V. I. Kuksa, V. A. Beylin, and R. S. Pasechnik, arXiv:hep-ph/0510036.

[14] V. Barger, C. W. Chiang, J. Jiang, and T. Li, Nucl. Phys. **B705**, 71 (2005); I. Antoniadis and S. Dimopoulos, Nucl. Phys. **B715**, 120 (2005); B. Bajc and G. Senjanovic, Phys. Lett. B **610**, 80 (2005); B. Kors and P. Nath, Nucl. Phys. **B711**, 112 (2005); K. Huitu, J. Laamanen, P. Roy, and S. Roy, Phys. Rev. D **72**, 055002 (2005); B. Dutta and Y. Mimura, Phys. Lett. B **627**, 145 (2005); A. Ibarra, Phys. Lett. B **620**, 164 (2005); V. Barger, J. Jiang, P. Langacker, and T. Li, Nucl. Phys. **B726**, 149 (2005); I. Antoniadis, A. Delgado, K. Benakli, M. Quiros, and M. Tuckmantel, Phys. Lett. B **634**, 302 (2006); C. Liu, Commun. Theor. Phys. **47**, 1088 (2007); I. Antoniadis, K. Benakli, A. Delgado, M. Quiros, and M. Tuckmantel, Nucl. Phys. **B744**, 156 (2006); N. Haba and N. Okada, Prog. Theor. Phys. **116**, 757 (2006); D. V. Gioutsos, G. K. Leontaris, and A. Psallidas, Phys. Rev. D **74**, 075007 (2006).

[15] S. h. Zhu, Phys. Lett. B **604**, 207 (2004); B. Mukhopadhyaya and S. SenGupta, Phys. Rev. D **71**, 035004 (2005); W. Kilian, T. Plehn, P. Richardson, and E. Schmidt, Eur. Phys. J. C **39**, 229 (2005); K. Cheung and W. Y. Keung, Phys. Rev. D **71**, 015015 (2005); D. A. Demir, arXiv:hep-ph/0410056; M. A. Diaz and P. F. Perez, J. Phys. G **31**, 563 (2005); S. P. Martin, K. Tobe, and J. D. Wells, Phys. Rev. D **71**, 073014 (2005); C. H. Chen and C. Q. Geng, Phys. Rev. D **72**, 037701 (2005); P. Gambino, G. F. Giudice, and P. Slavich, Nucl. Phys. **B726**, 35 (2005); K. Cheung and J. Song, Phys. Rev. D **72**, 055019 (2005); S. K. Gupta, B. Mukhopadhyaya, and S. K. Rai, Phys. Rev. D **73**, 075006 (2006); A. C. Kraan, J. B. Hansen, and P. Nevski, Eur. Phys. J. C **49**, 623 (2007).

[16] J. L. Hewett, B. Lillie, M. Masip, and T. G. Rizzo, J. High Energy Phys. 09 (2004) 070.

[17] A. Arvanitaki, S. Dimopoulos, A. Pierce, S. Rajendran, and J. G. Wacker, arXiv:hep-ph/0506242.

[18] N. Arkani-Hamed, S. Dimopoulos, G. F. Giudice, and A. Romanino, Nucl. Phys. **B709**, 3 (2005); D. Chang, W. F. Chang, and W. Y. Keung, Phys. Rev. D **71**, 076006 (2005); N. G. Deshpande and J. Jiang, Phys. Lett. B **615**, 111 (2005); G. F. Giudice and A. Romanino, Phys. Lett. B **634**, 307 (2006).

[19] U. Sarkar, Phys. Rev. D **72**, 035002 (2005); A. Datta and X. Zhang, Int. J. Mod. Phys. A **21**, 2431 (2006); K. S. Babu, T. Enkhbat, and B. Mukhopadhyaya, Nucl. Phys. **B720**, 47 (2005); M. Drees, arXiv:hep-ph/0501106; N. Haba and N. Okada, Prog. Theor. Phys. **114**, 1057 (2005); E. Dudas and S. K. Vempati, Nucl. Phys. **B727**, 139 (2005).

[20] L. Anchordoqui, H. Goldberg, and C. Nunez, Phys. Rev. D **71**, 065014 (2005).

[21] J. I. Illana, M. Masip, and D. Meloni, Phys. Rev. D **75**, 055002 (2007).

[22] G. R. Farrar and P. Fayet, Phys. Lett. **76B**, 575 (1978).

[23] P. F. Smith, J. R. J. Bennett, G. J. Homer, J. D. Lewin, H. E. Walford, and W. A. Smith, Nucl. Phys. **B206**, 333 (1982); T. K. Hemmick *et al.*, Phys. Rev. D **41**, 2074 (1990).

[24] A. Arvanitaki, C. Davis, P. W. Graham, A. Pierce, and J. G. Wacker, Phys. Rev. D **72**, 075011 (2005).

[25] D. J. Fixsen, E. S. Cheng, J. M. Gales, J. C. Mather, R. A. Shafer, and E. L. Wright, Astrophys. J. **473**, 576 (1996).

[26] D. N. Spergel *et al.*, Astrophys. J. Suppl. Ser. **170**, 377 (2007).

[27] P. Sreekumar *et al.* (EGRET Collaboration), Astrophys. J. **494**, 523 (1998); A. W. Strong, I. V. Moskalenko, and O. Reimer, arXiv:astro-ph/0306345.

[28] W. Hu and J. Silk, Phys. Rev. Lett. **70**, 2661 (1993); J. L. Feng, A. Rajaraman, and F. Takayama, Phys. Rev. D **68**, 063504 (2003).

[29] G. D. Kribs and I. Z. Rothstein, Phys. Rev. D **55**, 4435 (1997); **56**, 1822(E) (1997).

[30] F. Abe *et al.* (CDF Collaboration), Phys. Rev. D **46**, R1889 (1992).

[31] D. Acosta *et al.* (CDF Collaboration), Phys. Rev. Lett. **90**, 131801 (2003).

[32] D. Acosta (CDF Collaboration), Phys. Rev. Lett. **92**,

121802 (2004).
[33] V. M. Abazov *et al.* (D0 Collaboration), Phys. Rev. Lett. **99**, 131801 (2007).
[34] J. Abraham *et al.* (Pierre Auger Collaboration), Nucl. Instrum. Methods Phys. Res., Sect. A **523**, 50 (2004).
[35] J. G. Gonzalez, S. Reucroft, and J. Swain, Phys. Rev. D **74**, 027701 (2006).
[36] L. Anchordoqui, T. Paul, S. Reucroft, and J. Swain, Int. J. Mod. Phys. A **18**, 2229 (2003).
[37] K. Greisen, Phys. Rev. Lett. **16**, 748 (1966); G. T. Zatsepin and V. A. Kuzmin, Pis'ma Zh. Eksp. Teor. Fiz. **4**, 114 (1966) [JETP Lett. **4**, 78 (1966)].
[38] M. Roth (Pierre Auger Collaboration), arXiv:0706.2096; L. Perrone (Pierre Auger Collaboration), arXiv:0706.2643; P. Facal San Luis (Pierre Auger Collaboration), arXiv:0706.4322.
[39] D. V. Semikoz and G. Sigl, J. Cosmol. Astropart. Phys. 04 (2004) 003.
[40] G. R. Farrar, Phys. Rev. Lett. **76**, 4111 (1996); D. J. H. Chung, G. R. Farrar, and E. W. Kolb, Phys. Rev. D **57**, 4606 (1998).
[41] L. A. Anchordoqui, J. L. Feng, H. Goldberg, and A. D. Shapere, Phys. Rev. D **66**, 103002 (2002); N. G. Lehtinen, P. W. Gorham, A. R. Jacobson, and R. A. Roussel-Dupre, Phys. Rev. D **69**, 013008 (2004); P. W. Gorham, C. L. Hebert, K. M. Liewer, C. J. Naudet, D. Saltzberg, and D. Williams, Phys. Rev. Lett. **93**, 041101 (2004); M. Ackermann *et al.*, Astropart. Phys. **22**, 339 (2005); I. Kravchenko *et al.*, Phys. Rev. D **73**, 082002 (2006); O. B. Bigas (Pierre Auger Collaboration), arXiv:0706.1658.
[42] For a comprehensive discussion the reader is referred to A. C. Kraan, Eur. Phys. J. C **37**, 91 (2004).
[43] M. M. Block, F. Halzen, and T. Stanev, Phys. Rev. D **62**, 077501 (2000).
[44] J. Alvarez-Muniz, R. Engel, T. K. Gaisser, J. A. Ortiz, and T. Stanev, Phys. Rev. D **66**, 033011 (2002).
[45] D. Nitz (Pierre Auger Collaboration), arXiv:0706.3940.
[46] L. Anchordoqui, M. T. Dova, A. Mariazzi, T. McCauley, T. Paul, S. Reucroft, and J. Swain, Ann. Phys. (N.Y.) **314**, 145 (2004).
[47] S. J. Sciutto, AIRES User's Manual and Reference Guide, version 2.6.0 (2002), available electronically at www.fisica.unlp.edu.ar/auger/aires.
[48] National Aeronautics and Space Administration (NASA), National Oceanic and Atmospheric Administration (NOAA), and U.S. Air Force, U.S. Standard Atmosphere, NASA Technical Report No. NASA-TM-X-74335 and NOAA Technical Report No. NOAA-S/T-76-1562, 1976.
[49] A. Cillis and S. J. Sciutto, J. Phys. G **26**, 309 (2000).
[50] R. S. Fletcher, T. K. Gaisser, P. Lipari, and T. Stanev, Phys. Rev. D **50**, 5710 (1994); R. Engel, T. K. Gaisser, T. Stanev, and P. Lipari, Proc. ICRC **1**, 415 (1999).
[51] S. Ostapchenko, Nucl. Phys. B, Proc. Suppl. **151**, 143 (2006); N. N. Kalmykov, S. S. Ostapchenko, and A. I. Pavlov, Izv. Ross. Akad. Nauk Ser. Fiz. **58N12**, 21 (1994) [Bulletin of the Russian Academy of Sciences Physics **58**, 1966 (1994)].
[52] J. Knapp, D. Heck, S. J. Sciutto, M. T. Dova, and M. Risse, Astropart. Phys. **19**, 77 (2003).
[53] S. J. Sciutto (unpublished).
[54] L. A. Anchordoqui, M. T. Dova, L. N. Epele, and S. J. Sciutto, Phys. Rev. D **59**, 094003 (1999).
[55] A. N. Cillis, H. Fanchiotti, C. A. Garcia Canal, and S. J. Sciutto, Phys. Rev. D **59**, 113012 (1999).
[56] A. N. Cillis and S. J. Sciutto, Phys. Rev. D **64**, 013010 (2001).
[57] X. Bertou, P. Billoir, O. Deligny, C. Lachaud, and A. Letessier-Selvon, Astropart. Phys. **17**, 183 (2002).
[58] P. Hansen, P. Carlson, E. Mocchiutti, S. J. Sciutto, and M. Boezio, Phys. Rev. D **68**, 103001 (2003); P. Hansen, T. K. Gaisser, T. Stanev, and S. J. Sciutto, Phys. Rev. D **71**, 083012 (2005).
[59] L. Anchordoqui and H. Goldberg, Phys. Rev. D **65**, 047502 (2002).
[60] Note that because of the small inelasticity, the main characteristics of *R*-hadron air showers are independent of the external package used to process the high energy hadronic collisions.
[61] P. Facal San Luis *et al.*, Proc. ICRC **1**, 319 (2007).
[62] X. Bertou, P. Billoir, O. Deligny, C. Lachaud, and A. Letessier-Selvon, Astropart. Phys. **17**, 183 (2002).
[63] C. M. G. Lattes, Y. Fujimoto, and S. Hasegawa, Phys. Rep. **65**, 151 (1980).
[64] G. Arnison *et al.* (UA1 Collaboration), Phys. Lett. **122B**, 189 (1983).
[65] K. Alpgard *et al.* (UA5 Collaboration), Phys. Lett. **115B**, 71 (1982); G. J. Alner *et al.* (UA5 Collaboration), Phys. Lett. B **180**, 415 (1986).
[66] P. L. Melese (CDF Collaboration), Fermilab Report No. FERMILAB-CONF-96-205-E, 1996.